Applications of Integrated Geophysical Survey in Mapping Subsurface to a Depth of 80 ft at a Landfill in Salina, Kansas

Jianghai Xia and Richard D. Miller

Summary

Subsidence was observed at several places on the Salina Municipal Golf Course in areas known to be built over a landfill in Salina, Kansas. High-resolution magnetic survey (57,900 ft^2), multi-channel electrical resistivity profiling (three 504-ft lines), and microgravity profiling (23 gravity-station values) were performed on a subsidence site (Green 16) to evaluate the effectiveness of the geophysical methods in determining boundaries and density deficiency of the landfill in the vicinity of the subsidence. Horizontal boundaries of the landfill were confidently defined by both magnetic anomalies and the pseudo-vertical gradient of magnetic anomalies. Furthermore, the pseudo-vertical gradient of magnetic anomalies presented a unique anomaly at the surface of Green 16, which provided a criterion for predicting other spots with subsidence potential using the same gradient property. Results of multi-channel electrical resistivity profiling (ERP) suggested a bottom limit of the landfill at Green 16 was around 70 ft below the ground surface based on the vertical gradient of electric resistivity and *a priori* information on the depth of the landfill. ERP results also outlined several possible landfill bodies based on their low resistivity values. Microgravity results suggested a –0.14 g/cm^3 density deficiency at Green 16 that could equate to future surface subsidence as much as of 5 ft due to gradual compaction.

Introduction

Delineating or mapping a landfill has long been a challenge for near-surface geophysicists due to the complexity in the composition of subsurface materials. No single geophysical tool can effectively determine the characteristics of a landfill. Iterative and integrated data collection and interpretation using multiple geophysical methods provides for a more complete interpretation of data, often resulting in a more accurate model of the complex structures and processes of the subsurface (Dawson et al., 2002).

Subsidence was observed at Green 16 of the Salina Municipal Golf Course which was built over a landfill with few or no details concerning use and closure in Salina, Kansas (Figure 1a). High-resolution magnetic survey, electrical resistivity profiling (ERP), and microgravity profiling were used to delineate the subsidence around Green 16 (Figure 1b). Two photos (Figure 1c) taken in the directions of lines 1 and 3 show the general setting of the working site. Geophysical data were acquired and analyzed to obtain subsurface information on magnetic property, resistivity, and density.

The Kansas Geological Survey has a long history of using gravity and magnetic methods to solve regional geologic problems (Yarger, 1983, 1989; Lam and Yarger, 1989; Xia et al., 1992b, 1995a, 1995b, 1995c, 1996). Algorithms related to data processing and interpretation have been developed (Yarger et al., 1978; Xia et al., 1991,

1992a, 1993). Although this past research focused on deep (> 200 m) geology, the fundamentals of anomalies induced by the geomagnetic field in near-surface (< 30 m) materials remains the same. The successful brine well search and anomaly identification during the last three years in Hutchinson, Kansas, with the high-resolution magnetic method demonstrated its feasibility and advantages in mapping subsurface anomalies in an urban environment (Xia, 2002; Xia and Williams, 2003, 2004; Xia et al., 2003, 2004).

A high-resolution magnetic survey was performed in the area measuring approximately 57,900 ft^2 focusing on Green 16 and an area where Green 16 could potentially be moved. Magnetic anomalies horizontally delineated natural materials from the landfill residence. Magnetic gradient anomalies that defined Green 16 subsidence were used to predict other spots with similar magnetic properties.

Twenty-three microgravity-station values were measured along a line of 440 ft crossing Green 16. Microgravity anomalies suggested a density deficiency (–0.14 g/cm^3) in the area of Green 16. This density deficiency was used to estimate possible future subsidence due to compaction by utilization of results from ERP and an assumption based on the density of natural materials.

The purpose of two-dimensional (2D) electrical resistivity profiling is to determine the subsurface electric resistivity distribution by taking measurements along a survey line at the surface. A measurement in an electrical survey is normally composed of injecting electrical current into the ground through two current-carrying electrodes and measuring the resulting voltage difference at two potential electrodes. The apparent resistivity is calculated using the injected current, the voltage measured, and a geometric factor related to the arrangement of the four electrodes (Zohdy et al., 1974; Reynolds, 1997). The investigation depth of electrical resistivity depends generally on the spacing between the electrodes that inject electrical current. Therefore, sampling at different depths can be done by changing the spacing between the electrodes. Measurements are repeated along a survey line with various combinations of electrodes and spacing to produce an apparent resistivity cross-section.

Apparent resistivity data are then inverted to generate a model of the subsurface structure and stratigraphy based on its electrical properties (Wolfe et al, 2000, deGroot-Hedlin and Constable, 1990; Oldenburg and Li, 1999; Tsourlos et al., 1999; Loke, 2001). Many geological/environmental or cultural factors affect or control the resistivity of the subsurface such as composition of the subsurface materials, amount of water in the subsurface, and ionic concentration of the pore fluid. A resistivity model can be used to identify, delineate, and map subsurface features such as electrically conductive contamination plumes, bedrock fracture zones, the saltwater/freshwater interface, the vadose zone, electrically conductive lithologic units such as clay, and sediment size distribution (Dawson et al., 2002; Behiry and Hanafy 2000; Benson et al., 1997).

The ERP survey was performed along three 504-ft lines. Two of three lines crossed Green 16, one in the west-east and one in the south-north direction. A third line was located 100 ft west of Green 16 in the south-north direction. Measured apparent

resistivity data were inverted into resistivity models. From these models, we were able to define bodies of landfill materials and the bottom limits of the landfill with resistivity models based on landfill history.

Data Acquisition

Grids and lines

We used a CST/Berger electronic digital theodolite (Figure 2) to define the survey area (x, y), three survey lines, and elevation (z) of line 1 (Figure 1b). High-resolution magnetic data were acquired in an area measuring 57,900 ft^2. The survey area was divided into 2 grids: the first was 270 ft × 170 ft and the second 120 ft × 100 ft (Figure 1b). Electrical resistivity profiling was performed along three 504-ft lines. Line 1 was laid out in the east-west direction on the top of the landfill; lines 2 and 3 were perpendicular to line 1 (Figure 1b). A microgravity survey was also performed along line 1 (Figure 1b and 1c).

Magnetic survey

A Geometrics G858 portable cesium gradiometer (Figure 3) was used to perform a high-resolution magnetic survey by measuring the total component of the geomagnetic field and the vertical gradient of the geomagnetic field. The bottom and top sensor heights were 16 in and 36 in above the ground surface, respectively, over the entire survey area. The magnetic data were acquired along lines at 3 ft spacing (Figure 4) and an average measurement density of 2.3 measurements/ft. During the magnetic data acquisition, the other Geometrics G856 Proton magnetometer was used to measure the diurnal changes of the earth field every 10 minutes on a fixed station around 200 ft away from the survey area (Figure 5). The maximum diurnal change during the survey period of time was around 12 nT (Figure 6). The normal geomagnetic field in Salina was 53,540 nT. We expected the high-resolution magnetic survey could provide data with sufficient resolution to define horizontal boundaries between the landfill and natural materials.

Resistivity survey

Electrical resistivity profiling (ERP) was performed along three 504-ft lines using a Geopen™ E60C multi-electrode resistivity meter (Figure 7a) with 64 electrodes (Figure 7b). Electrode spacing was set at 8 ft. The main purpose of the ERP survey was to delineate the bottom of the landfill. Line 1 was laid out in the east-west direction on the top of the landfill (Figure 1b). Two other lines were perpendicular to line 1. The Wenner array (Figure 8) was used in the ERP. The resistivity meter systematically and automatically selects current electrodes and measurement electrodes to sample. The investigation depth increases with increasing distance between electrodes. The maximum investigation depth for this array was around 80 ft to 100 ft (1/6 to 1/5 of the profile length).

Microgravity survey

The microgravity survey was conducted along line 1 with a station spacing of 20 ft using the LaCoste & Romberge D-71 meter (Figure 9) in hopes of determining

density differences between the landfill and natural materials. The first station (at 60 ft) was designated as the base station. All gravity readings started and ended at the base station. Microgravity readings were taken at 23 stations.

Data Processing

Magnetic data

Magnetic data were processed using the following procedure.

1) Assignment of field geometry.
2) Correction for the sensor locations based on shapes of linear anomalies due to ridges in the survey area by shifting odd numbered lines by 0.5 ft – 1.4 ft.
3) The diurnal correction was applied based on the base station readings (Figure 6).
4) Merging data of two grids into one file.
5) Gridding data by a linear Kriging method with a search radius of 6 ft. Measurements were then gridded into 1 ft × 1 ft grids (Surfer®, 1999). Three data sets were generated: the total field component of magnetic anomaly from the bottom sensor, the top sensor, and the pseudo-vertical gradient of magnetic anomaly (= readings from the bottom sensor – readings from the top sensor).
6) Display of high-resolution magnetic data using Surfer® in a color scale to enhance anomalies.

The total field component of magnetic anomaly from the top sensor, the bottom sensor, and the pseudo-vertical gradient of magnetic anomaly (= readings from the bottom sensor – readings from the top sensor) are shown in Figures 10a, 10b, and 10c, respectively.

Resistivity data

Measured apparent resistivity data were inverted using EarthImager™ (AGI, 2005). We selected the smooth model inversion algorithm. The measured apparent resistivity data were in the range of 1 to 30 Ohm-m except for measurements around station 144 ft of line 3 where readings were over 2,700 Ohm-m. These higher readings were due to a pipe in the sprinkler system. To invert the measured apparent resistivity data of line 3 for the subsurface model, we removed data that were over 50 Ohm-m before inversion. Figures 11a, 12a, and 13a are measured apparent resistivity data used as inputs for the inversion. The original measured data of line 3 are shown in Figure 13d. Figures 11b, 12b, and 13b are calculated apparent resistivity data based on the inverted resistivity models shown in Figures 11c, 12c, and 13c, respectively. Calculated apparent resistivity data generally fit the measured apparent resistivity data.

Microgravity data

Microgravity data (Figure 14a) were processed using the following procedure.

1) The meter drift correction and the tidal correction were performed by linear distribution of the difference between two base station readings.
2) The elevation correction and the Bouguer correction were calculated using the following formula

$$f = (0.3086 - 0.0419\rho)h$$

where ρ is the average density of surface materials and in g/cm^3, and *h* is the elevation relative to the base station (Figure 14b) and in meters. Since the net effect is negative, i.e., higher station has lower gravity, the correction is positive, and the higher the station, the greater the correction to be added. Values of *f* are in mGal and depend on values of density ρ. We used 1.8 g/cm^3 in our corrections. Corrected data are shown in Figure 15a.

3) A regional gravity anomaly was assumed to be linear and modeled by a linear fitting algorithm (Grapher®, 2004).
4) A residual anomaly (Figure 15b) was calculated by subtracting the regional anomaly from corrected data (Figure 15a) and smoothed by a three-point-moving-average filter (0.25, 0.5, 0.25).

Data Interpretation

Magnetic data

In the following discussion, we define Grid East as the x-axis and Grid North as the y-axis. Two linear trends of magnetic highs (dashed lines) around lines y = 200 ft and y = 300 ft in the east-west direction from the top sensor (Figure 16a) and the bottom sensor (Figure 16b) clearly define two ridges (natural materials). The magnetic highs are interpreted here as characteristic of the natural materials. The linear magnetic high along y = 300 ft stops (A in Figures 16a and 16b) from x = 220 ft to x = 270 ft, which indicate possible locations of fill materials.

Besides two linear anomalies, the pseudo-vertical gradient of the magnetic anomaly shows values of -100 to -200 nT at the southeast corner of Green 16 (* in Figure 16c) where the ground is unsettled. We identified another spot along line 1 that possesses the same magnetic characteristics as * on Green 16: x = 120 ft (A in Figure 16c). We have also determined another location, x = 145 ft and y = 365 ft (B in Figure 16c), where the magnetic characteristics are very similar to those observed at location * on Green 16.

Resistivity data

Line 1 crossed Green 16 in the east-west direction with the center of the line located at the center of the green. Information on the landfill suggested that it was around 60 ft deep. The maximum gradient of geophysical properties often occurs at an interface between different materials. Based on this information and geophysical characteristics, we delineated the bottom limit of the landfill along the line 1 (Figure 17a).

A low resistivity body beneath Green 16 indicated that the overall volume containing landfill materials possesses a relatively low resistivity compared with the natural or native materials. This could be due to landfill materials or high water content in these spaces because of the relatively low density (high porosity) these materials possess. Several potential landfill bodies are outlined with dashed lines. Because of the measurement characteristic of this method, the apparent discontinuous nature of these bodies could be misleading. The discontinuous bodies of the landfill interpreted based on the resistivity model may be due to the resolution of the method. The landfill materials could be continuous along the section of line 1 in the real world. Nevertheless, the

outlined spots possess low resistivity and less compacted materials and a high likelihood of subsidence prone areas in the future.

The interpreted sections of lines 2 and 3 are shown in Figures 17b and 17c. The centers (252 ft) of lines 2 and 3 were tied at 130 ft and 230 ft of line 1. The bottom limits of the landfill at the tie points agree extremely well and provide the reference for extrapolations between these two lines.

Several possible landfill bodies are outlined by dashed lines based on their relatively low resistivity (in blue). They possess the same magnetic characteristics. Two are along line 1. The first is around station 288 (* in Figure 16c) where the ground is unsettled. The second is at around station 96 (A in Figure 16c). Two bodies along line 2 are at around stations 250 and 365 (A and B in Figure 16c). Relatively high resistivity centered at station 60, 184, 308, and 410 at the surface along line 2 (Figure 17b) was determined to be due to natural materials (ridges). Line 3 (Figure 17c), parallel to line 2, possesses similar characteristics as line 2 except there is no resistivity high around station 300. Values of resistivity around station 300 support the suggestion by the magnetic results that there could be landfill materials at that location (the same as A in Figure 16b).

Microgravity data

The general shape of the residual anomaly approximately mimics the interpreted bottom limit of the landfill along line 1 interpreted from the resistivity model (Figure 17a). This suggests that the residual anomaly is mainly due to the landfill and it is reasonable to model the regional gravity field with a linear trend analysis. The residual anomaly (Figure 14b) from stations 260 ft to 340 ft shows the maximum negative anomaly is approximately 0.04 mGal. The gravity low is associated with the unsettled location (* in Figure 16c).

Based on the bottom limit of the landfill along line 1 (Figure 17a), an average depth between stations 240 ft and 280 ft is approximately 70 ft. A spherical model with a diameter of 70 ft and a density contrast of –0.14 g/cm^3 possesses a maximum negative anomaly of 0.041 mGal. The density deficiency (–0.14 g/cm^3) can be used to estimate the maximum future subsidence due purely to compaction. The density of natural materials is assumed to be 1.8 g/cm^3 so the maximum subsidence would be 7.7% (0.14/1.8) of 70 ft or 5.4 ft. Obvious changes in the density of natural materials will change the estimation of the maximum subsidence. For example, if the density of natural materials is assumed to be 1.6 g/cm^3 or 2.0 g/cm^3, the maximum subsidence would be 6.1 ft or 4.9 ft, respectively. The maximum theoretical subsidence in the future, therefore, should be in the range of 5 to 6 ft.

Conclusions and Recommendations

The geophysical characteristics at the unsettled spot of Green 16 (* in Figure 18) are relatively low in magnetic susceptibility and the pseudo-vertical gradient of -100 to -200 nT, relatively low in resistivity, and –0.14 g/cm^3 in the density deficiency. Estimation based on a spherical model suggests that a maximum theoretical subsidence of

5 to 6 ft is possible at Green 16 in the future due purely to gradual compaction. In practice, a most likely scenario is about one half of this maximum subsidence (2 to3 ft) would occur if there is no subsurface erosion (landfill materials washed away by ground water). Based on the observation of surface-water movement, subsurface erosion could occur at the southeast corner of Green 16 (* in Figure 18), which could increase both a rate and a magnitude of the future subsidence.

A candidate for replacement of Green 16 should possesses geophysical characteristics opposite of Green 16. A dashed ellipse in Figure 18 outlines a potential candidate for replacement of Green 16. This spot possesses relative high resistivity (station 312 ft on line 2), high magnetic susceptibility (Figures 16a and 16b), and over 1,000 nT of the pseudo-vertical gradient.

Acknowledgements

Mark Lytle of the City of Salina provided assistance and arrangements for the data acquisition. Field assistants were Ryan Rutherford and August Johnson of Kansas Geological Survey.

References

AGI, 2005, EarthImager, 2D resistivity and IP inversion software: Advanced Geosciences, Inc.

Behiry, M.G., and Hanafy, S.M., 2000, Geophysical surveys to map the vertical extension of a sinkhole: a Comparison Study: Symposium on the Application of Geophysics to Engineering and Environmental Problems (SAGEEP-2000, Arlington, VA, Feb. 2000), Powers, et al, eds., Environmental and Engineering Geophysical Society, 341-350.

Benson, A.K., Payne, K., and Stubben, M.A., 1997, Mapping groundwater contamination using dc resistivity and VLF geophysical methods–A case study: Geophysics, 62, 80-86.

Dawson, C.B., Lane, J.W., Jr., White, E.A., and Belaval, M., 2002, Integrated geophysical characterization of the Winthrop landfill southern flow path, Winthrop, Maine: Symposium on the Application of Geophysics to Engineering and Environmental Problems (SAGEEP) 2002 Annual Meeting of EEGS, Las Vegas, Nevada, February 10-14, 2002, available on CD.

deGroot-Hedlin, C., and Constable, S., 1990, Occam's Inversion to generate smooth, two-dimensional models from magnetotelluric data: Geophysics, 55, 1613-1624.

Grapher®, 2004, User's guide: Golden Software, Inc.

Lam, C.K., Yarger, H.L., 1989, State gravity map of Kansas: *in* Geophysics in Kansas edited by Don W. Steeples, Kansas Geological Survey Bulletin 226, p. 185-196.

Loke, M.H., 2001, Tutorial: 2-D and 3-D electrical imaging surveys. http://www.geoelectrical.com (accessed 13 Mar. 2001).

Oldenburg, D.W., and Li, Y., 1999, Estimating depth of investigation in DC resistivity and IP surveys: Geophysics, 64, 403-416.

Reynolds, J.M., 1997, An introduction to applied environmental geophysics, West Sussex, England, John Wiley & Sons Ltd., 796 p.

Surfer®, 1999, User's guide: Golden Software, Inc.

Tsourlos, P.I., Szymanski, J.E., and Tsokas, G.N., 1999, The effect of terrain topography on commonly used resistivity arrays: Geophysics, 64, 1357-1363.

Wolfe, J.P, Richard, H., Hauser, E., and Hinks, J., 2000, Identifying potential collapse zones under highways: in Proceedings: Symposium on the Application of Geophysics to Engineering and Environmental Problems (SAGEEP-2000, Arlington, Virginia February 20-24), Environmental and Engineering Geophysical Society, pp. 351-358.

Xia, J., and Sprowl, D.R., 1991, Correction of topographic distortions in gravity data: Geophysics, 56, 537-541.

Xia, J., and Sprowl, D.R., 1992a, Inversion of potential field data by iterative forward modeling in the wavenumber domain: Geophysics, 57, 126-130.

Xia, J., Yarger, H., Lam, C., Steeples, D.W., and Miller, R.D., 1992b, Bouguer gravity map of Kansas: Kansas Geological Survey Map Series, M-31.

Xia, J., Sprowl, D.R., and Adkins-Heljeson, D., 1993, Correction of topographic distortions in potential-field data: a fast and accurate approach: Geophysics, 58, 515-523.

Xia, J., Miller, R.D., and Steeples, D.W., 1995a, Aeromagnetic map of Kansas, reduced to the pole with second vertical derivative calculated: Kansas Geological Survey Map Series, M-41A.

Xia, J., Miller, R.D., and Steeples, D.W., 1995b, Bouguer gravity map of Kansas, second vertical derivative calculated: Kansas Geological Survey Map Series, M-41B.

Xia, J., and Sprowl, D.R., 1995c, Moho depths in Kansas from gravity inversion assuming exponential density contrast: *Computers & Geosciences*, 21, 237-244.

Xia, J., Sprowl, D.R., and Steeples, D.W., 1996, A model of Precambrian geology of Kansas from gravity and magnetic data: *Computers & Geosciences*, 22, 883-895.

Xia, J., 2002, Using electromagnetic methods to locate abandoned brine wells in Hutchinson, Kansas: Symposium on the Application of Geophysics to Engineering and Environmental Problems (SAGEEP) 2002 Annual Meeting of EEGS, Las Vegas, Nevada, February 10-14, 2002, 11 pp, available on CD.

Xia, J., and Williams, S.L., 2003, High-resolution magnetic survey in locating abandoned brine wells in Hutchinson, Kansas: Symposium on the Application of Geophysics to Engineering and Environmental Problems (SAGEEP) 2003 Annual Meeting of EEGS, April 6-10, 2003, San Antonio, Texas, 12 pp, available on CD.

Xia, J., Chen, C., Xia, S. and Laflen, D., 2003, Applications of High-resolution Magnetic Method and Gradient Method in Locating Abandoned Brine Wells in Hutchinson, Kansas: Kansas Geological Survey Open-file Report 2003-48, 150 pp.

Xia, J., and Williams, S.L., 2004, High-resolution magnetic survey used in searching for buried brine wells in Hutchinson, Kansas: *in* Johnson, K.S. and Neal, J.T. (eds.), Evaporate Karst and Engineering and Environmental Problems in the United States, *Oklahoma Geological Survey Circular* 109, 169-175.

Xia, J., Chen, C., Xia, S., Laflen, D., and Williams, S.L., 2004, Using high-resolution magnetic method and gradient method to locate abandoned brine wells in Hutchinson, Kansas: Symposium on the Application of Geophysics to

Engineering and Environmental Problems (SAGEEP) 2004 Annual Meeting of EEGS, February 22-26, Colorado Springs, Colorado, 1350-1367, also available on CD.

Yarger, H.L., Robertson, R.R., and Wentland, R.L., 1978, Diurnal drift removal from aeromagnetic data using least squares: Geophysics, 43, 148-156.

Yarger, H.L, 1983, Regional interpretation of Kansas aeromagnetic data: Kansas Geological Survey, Geophysics Series 1, p. 1-35.

Yarger, H.L., 1989, Major magnetic features in Kansas and their possible geological significance: *in* Geophysics in Kansas edited by Don W. Steeples, Kansas Geological Survey Bulletin 226, p. 197-213.

Zohdy, A.A.R., Eaton, G.P., and Mabey, D.R., 1974, Application of surface geophysics to ground-water investigations: Techniques of Water-Resources Investigations of the United States Geological Survey, book 2, chap. D1, 116 p.

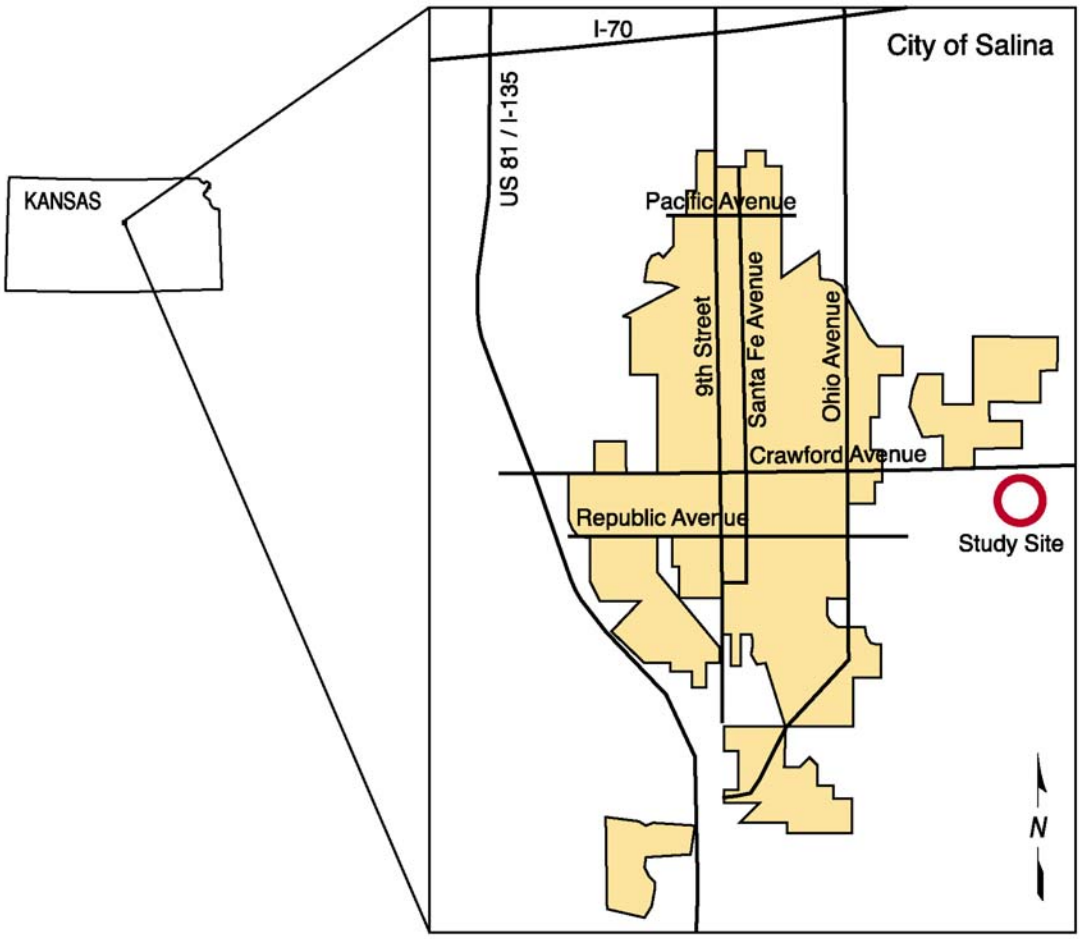

Figure 1a. The geographic location of the study site.

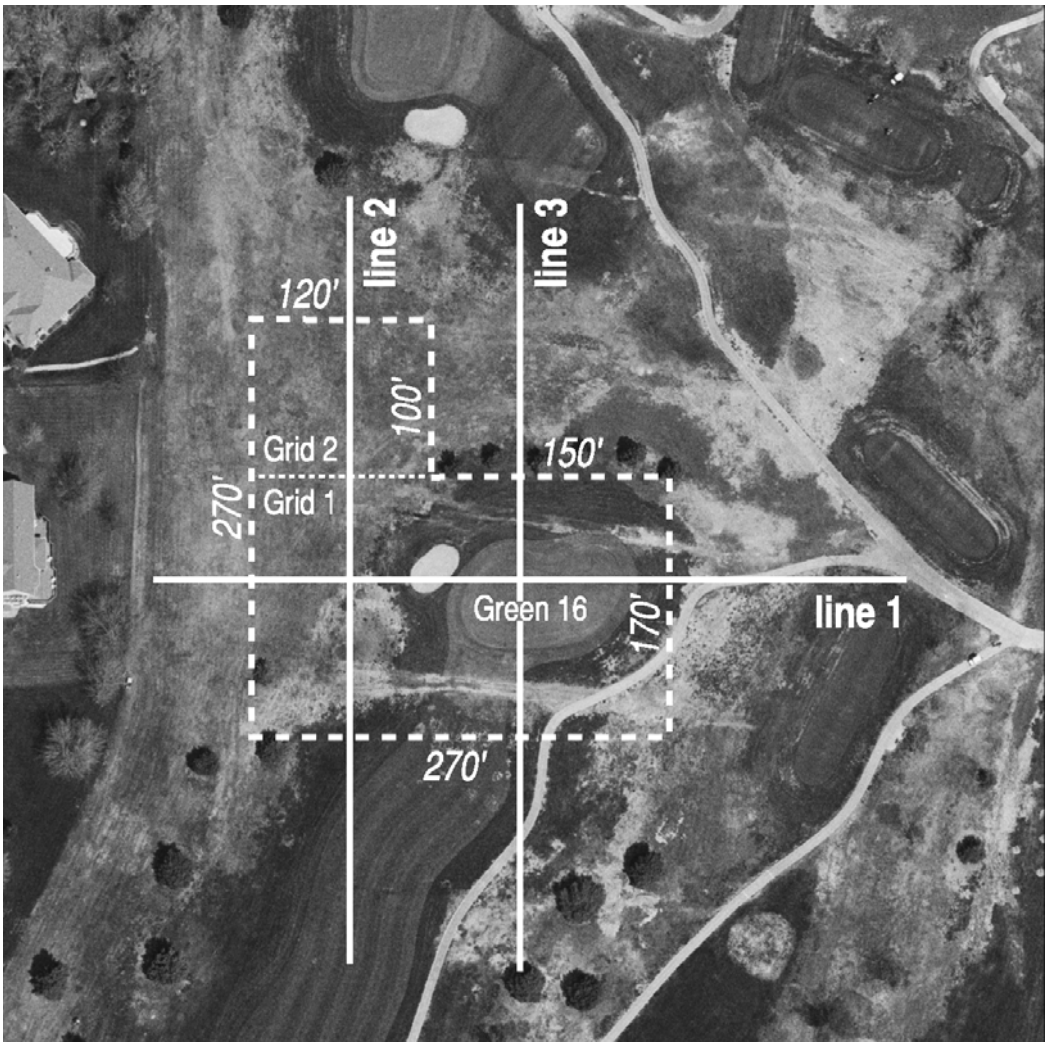

Figure 1b. Site map of the study area. A high-resolution magnetic survey was performed in the area outlined by dashed lines. Electric resistivity profiling was performed along three lines. Microgravity was measured along line 1.

Figure 1c. The view to the east from the west end of line 1 (left). The camera was pointed to the north from the south end of line 3 (right).

Figure 2. A CST/Berger electronic digital theodolite was used in defining grids, lines, and elevations along line 1.

Figure 3. A portable cesium gradiometer G858 was used to measure the total component of the geomagnetic field.

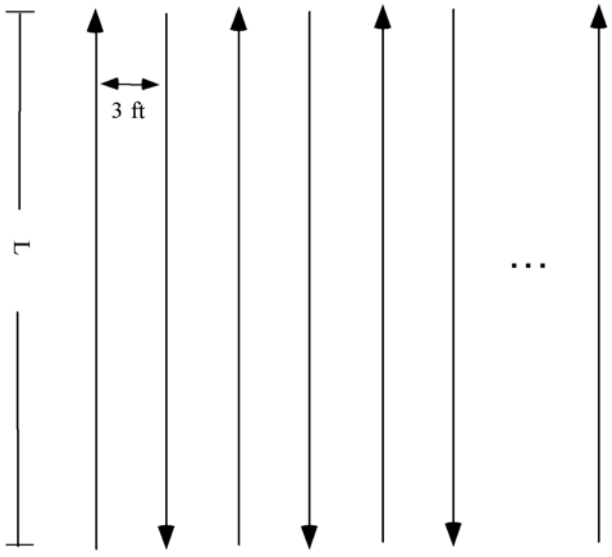

Figure 4. Survey lines within a grid. Arrows indicate the walking direction. Line 1ength L was 170 ft for grid 1 and 100 ft for grid 2.

Figure 5. A Geometrics G856 proton magnetometer was used to measure the diurnal changes of the geomagnetic field.

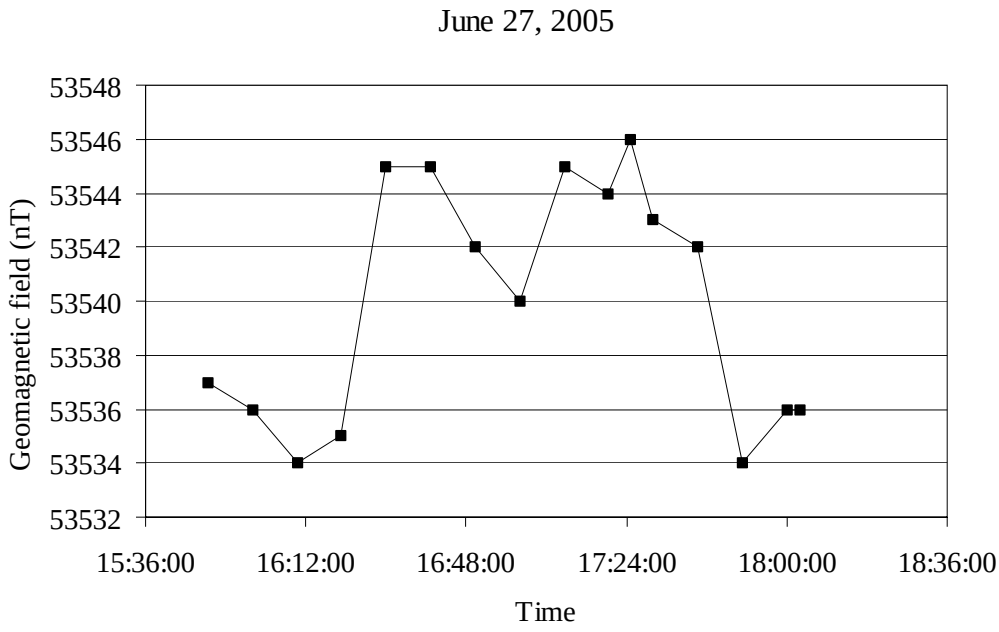

Figure 6. The diurnal changes of the geomagnetic field at the study site on June 27, 2005. The data were used for the diurnal correction.

Figure 7a. A Geopen^{TM} E60C multi-electrode resistivity meter was used in ERP survey.

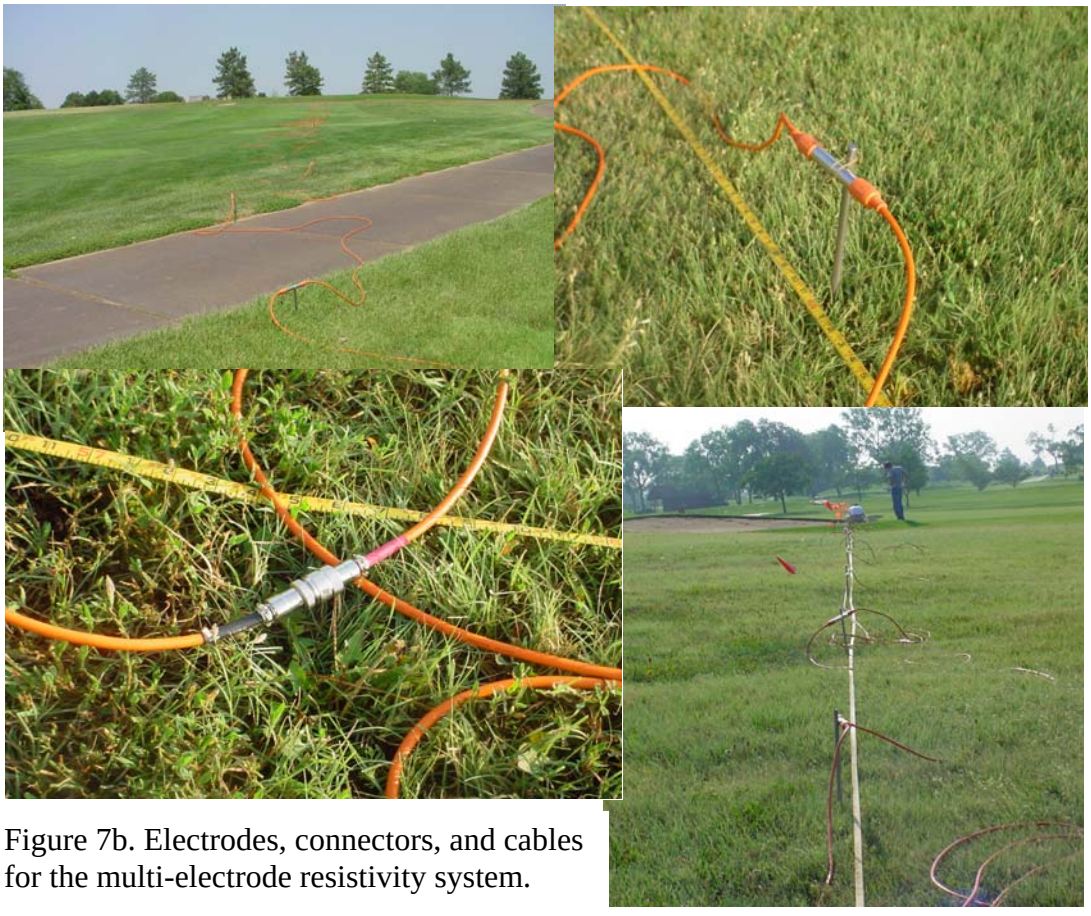

Figure 7b. Electrodes, connectors, and cables for the multi-electrode resistivity system.

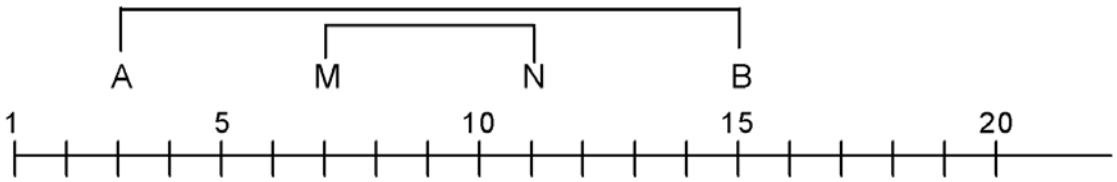

Figure 8. The Wenner array, where AM = MN = NB. Electrodes A and B are the current electrodes. Electrodes M and N are measurement electrodes. As the array moves along a line and changes the distance between electrodes, a resistivity meter is measuring apparent resistivity at different locations and depths, respectively.

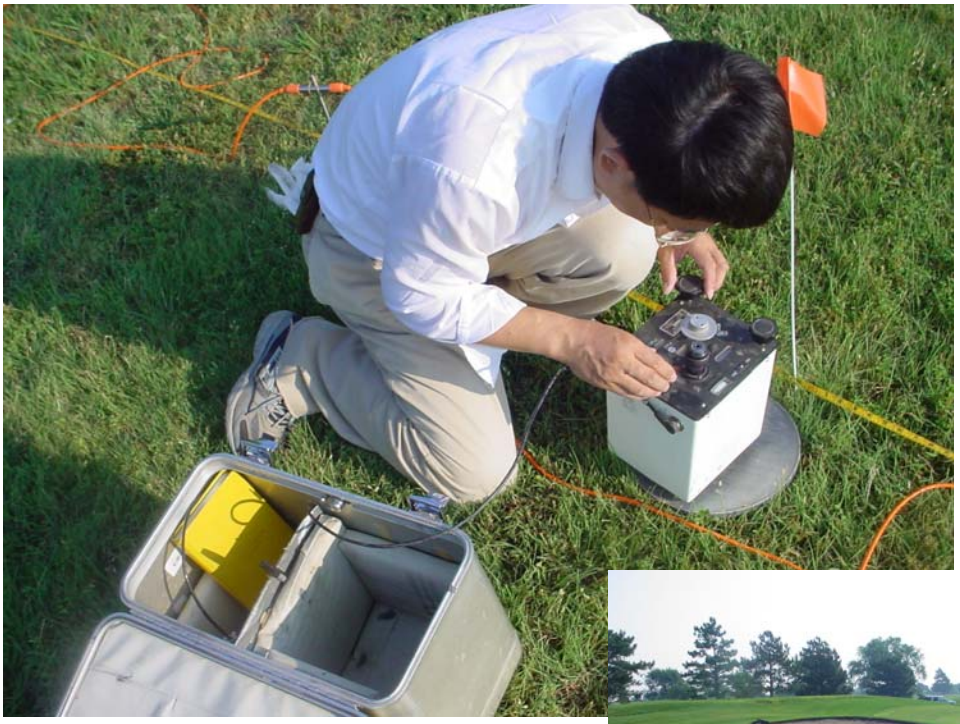

Figure 9. The LaCoste & Romberge D-71 meter was used in the microgravity survey.

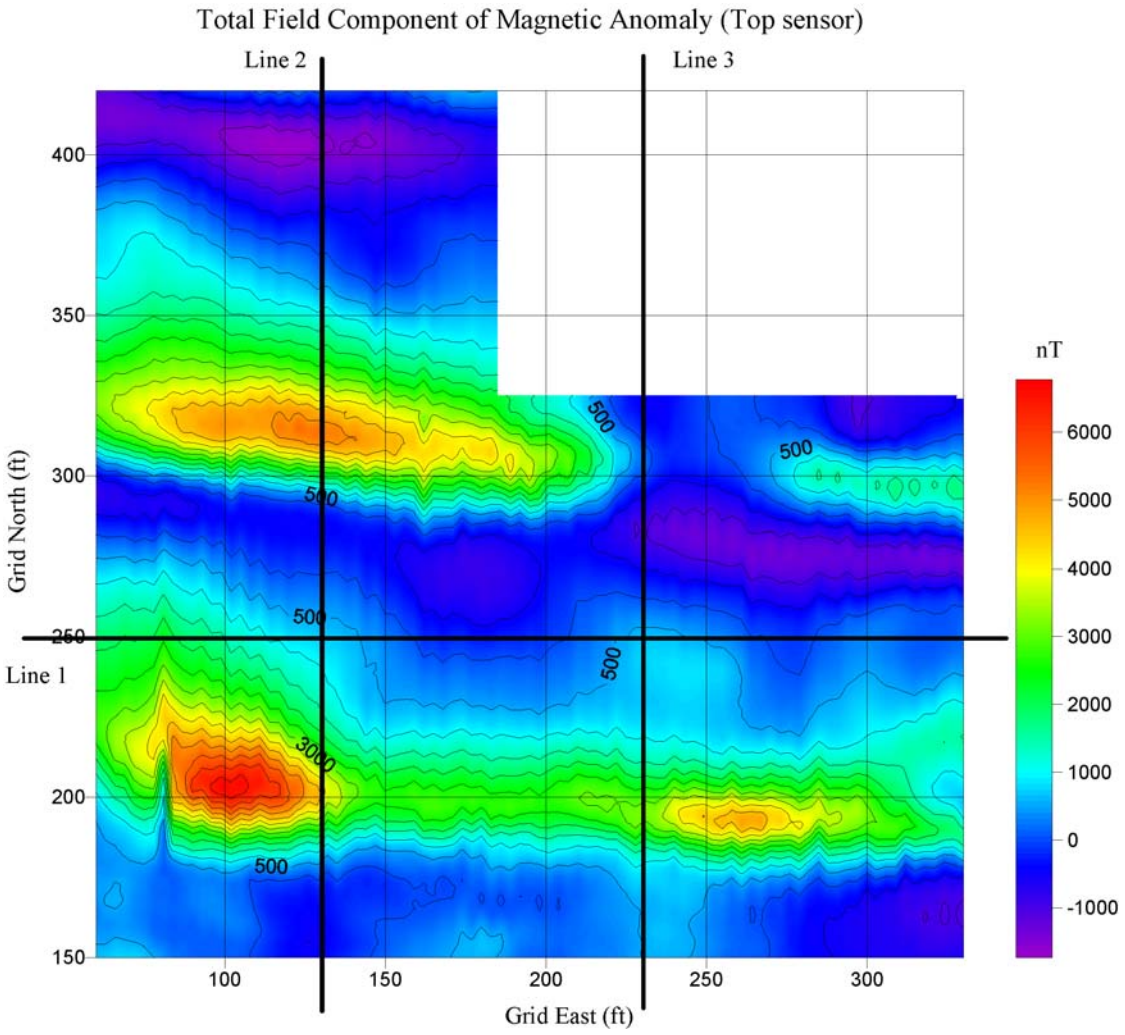

Figure 10a. The total field component of magnetic anomaly from the top sensor.

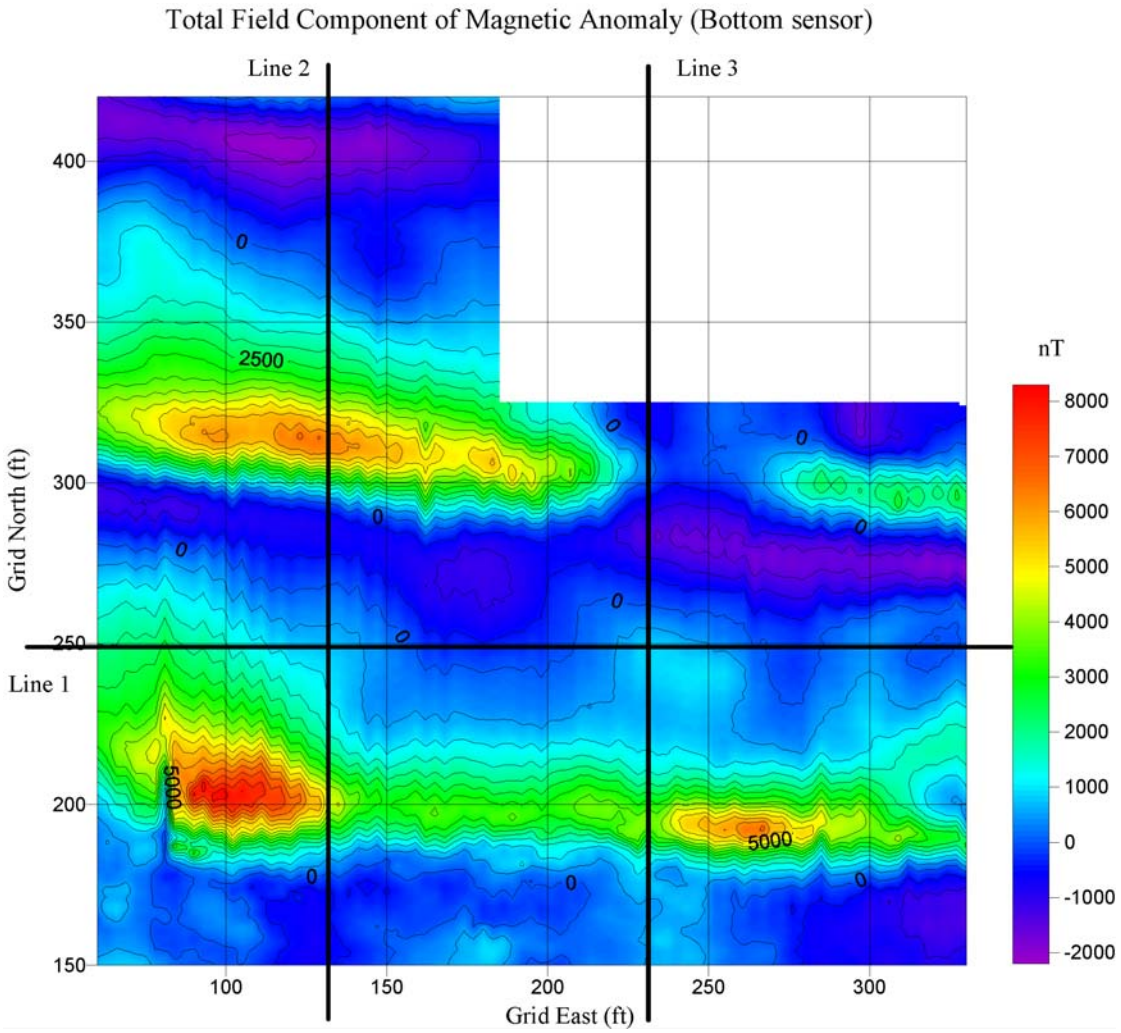

Figure 10b. The total field component of magnetic anomaly from the bottom sensor.

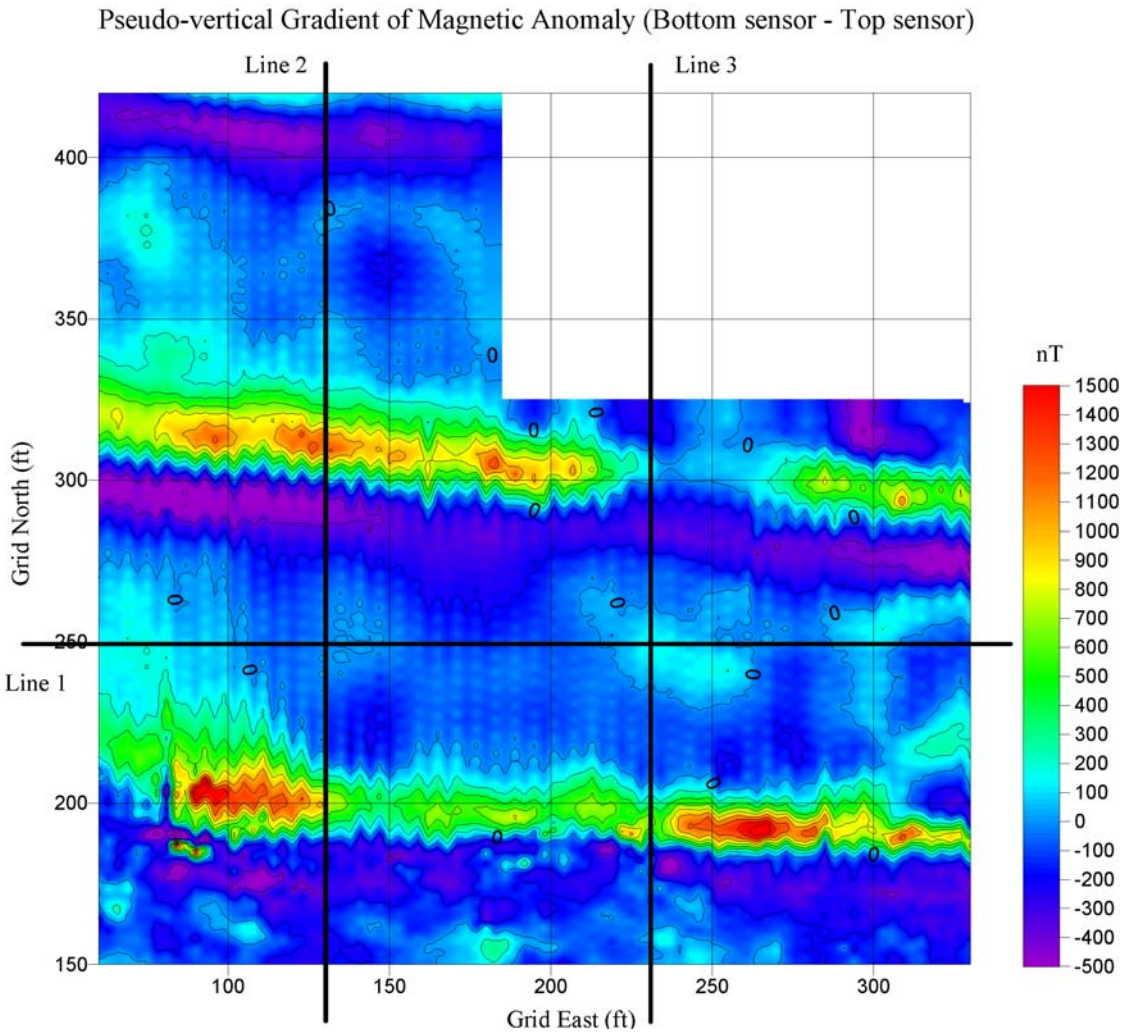

Figure 10c. The pseudo-vertical gradient of magnetic anomaly.

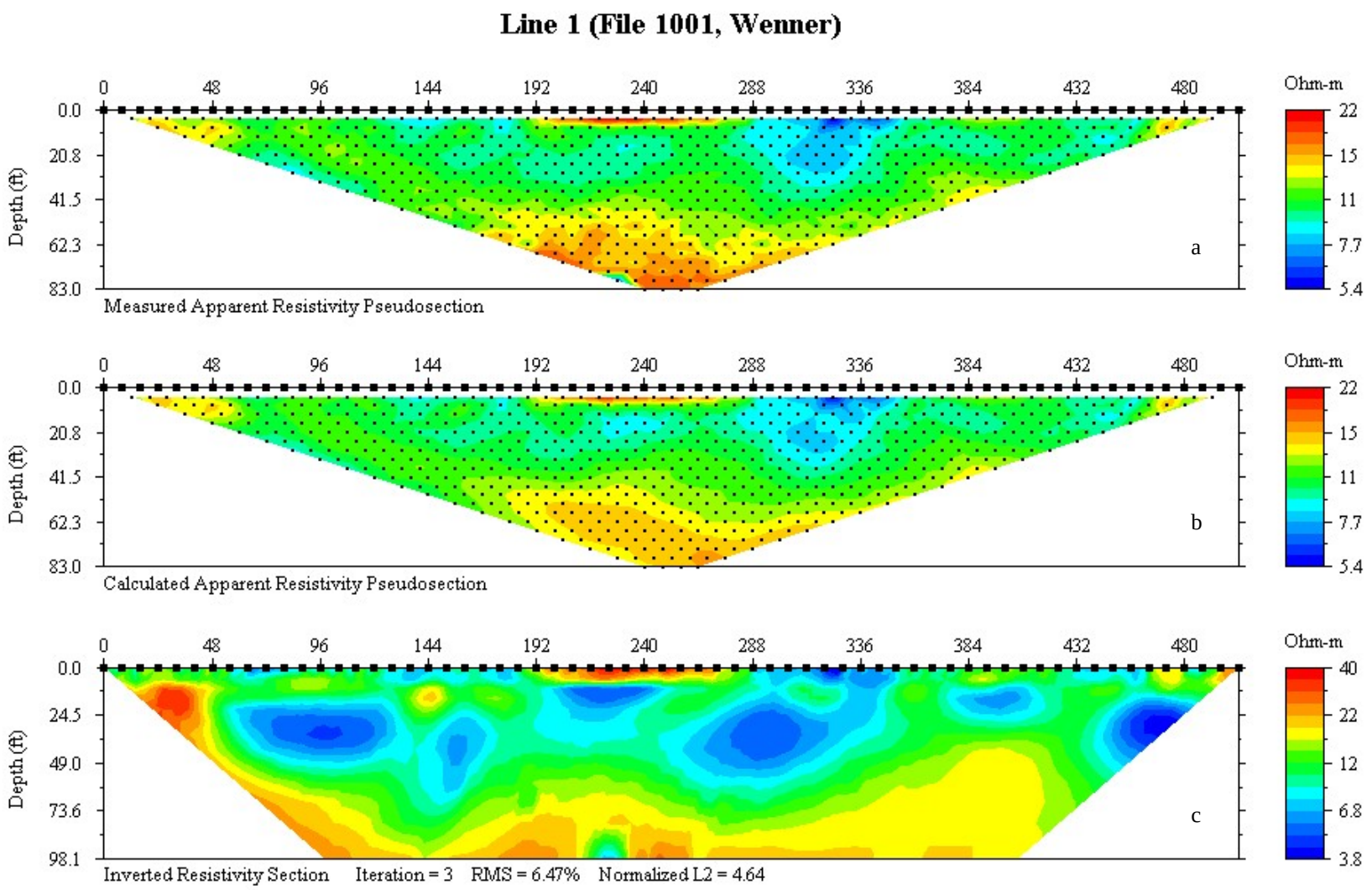

Figure 11. ERP results of line 1. (a) Measured apparent resistivity. Solid squares represent electrodes and dots are data points. (b) Calculated apparent resistivity data based on the inverted resistivity models shown in (c). (c) The inverted resistivity model.

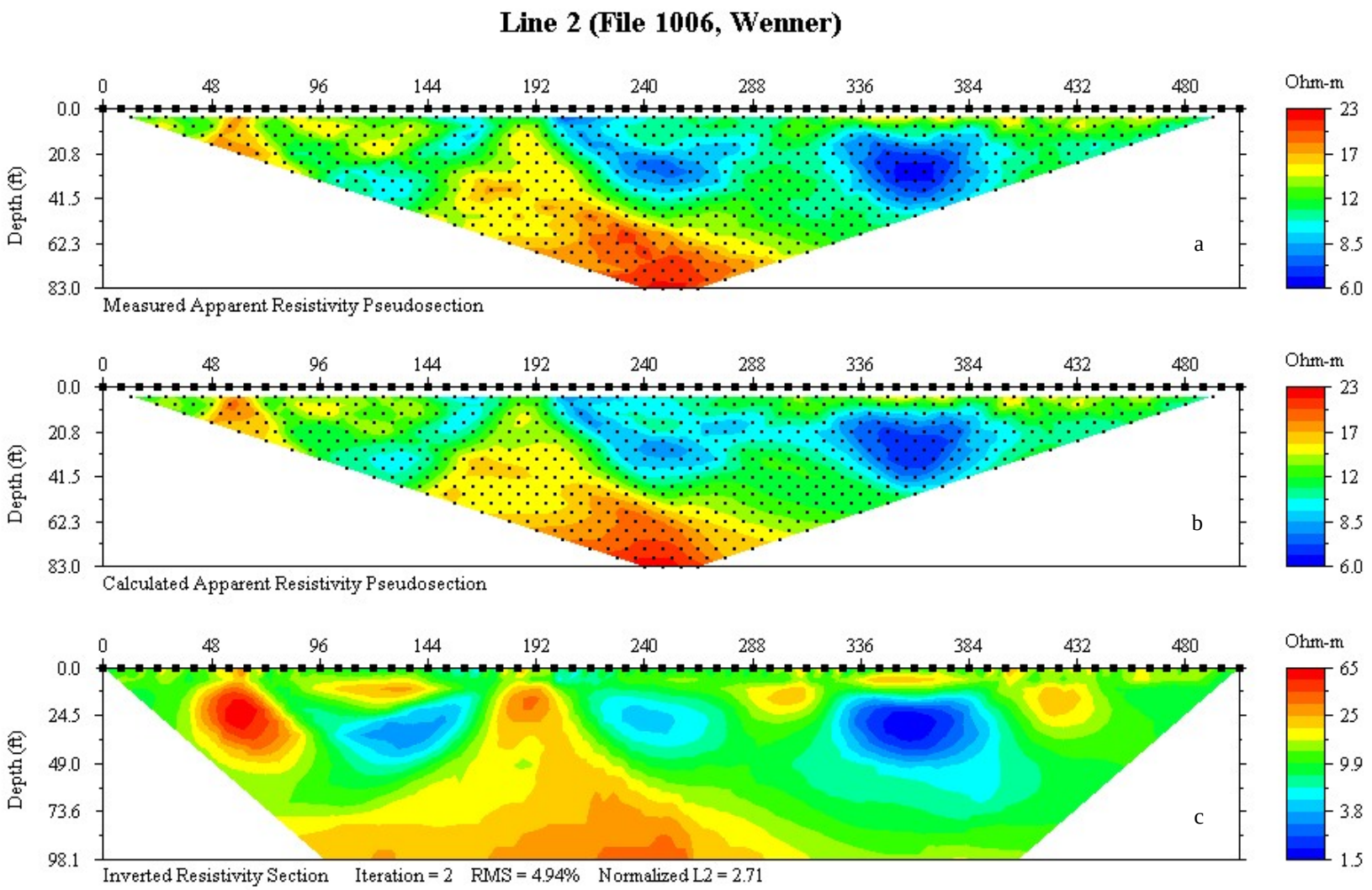

Figure 12. ERP results of line 2. (a) Measured apparent resistivity. Solid squares represent electrodes and dots are data points. (b) Calculated apparent resistivity data based on the inverted resistivity models shown in (c). (c) The inverted resistivity model.

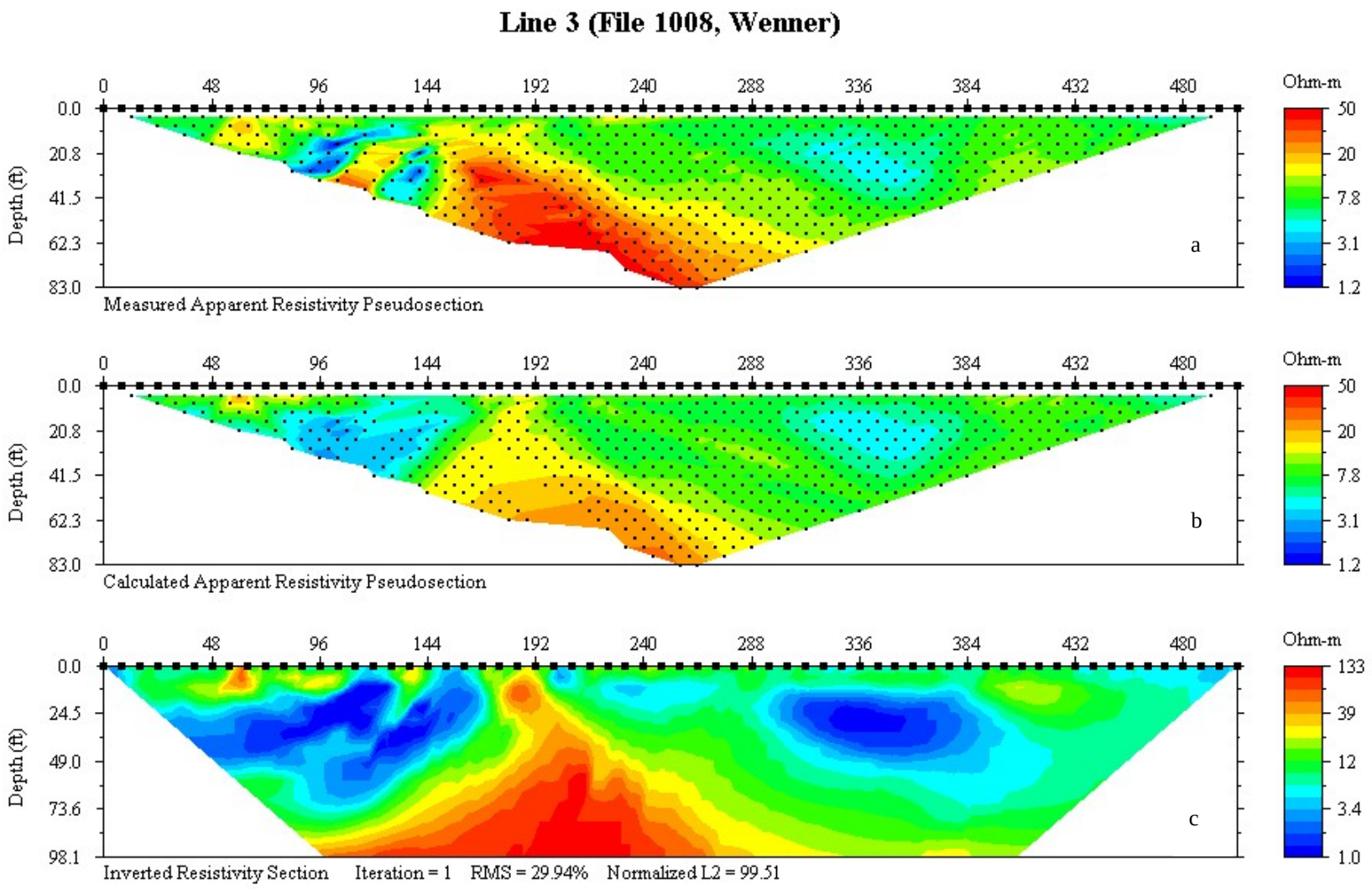

Figure 13. ERP results of line 3. (a) Measured apparent resistivity with removal of readings over 2,700 Ohm-m. Solid squares represent electrodes and dots are data points. (b) Calculated apparent resistivity data based on the inverted resistivity models shown in (c). (c) The inverted resistivity model.

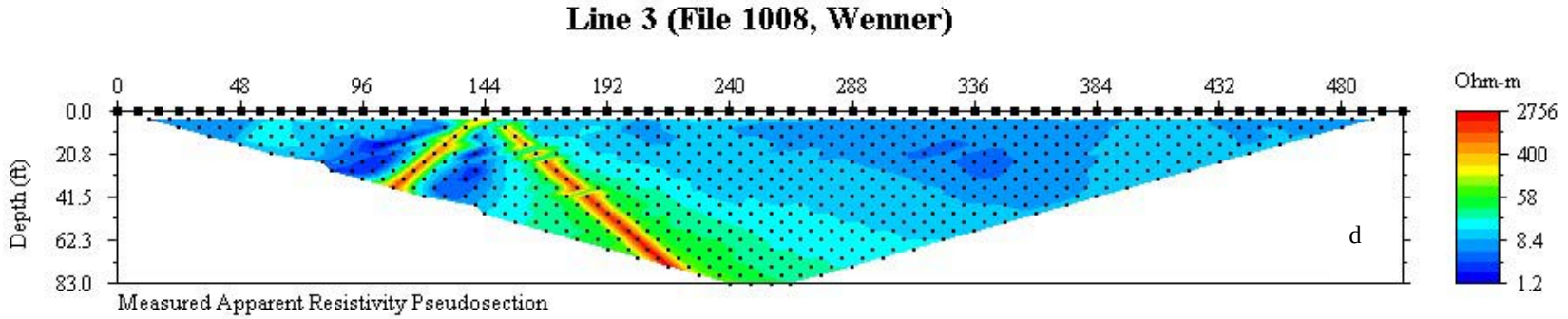

Figure 13d. Measured apparent resistivity of line 3. High readings around station 144 ft were due to a pipe of sprinkle system. Solid squares represent electrodes and dots are data points.

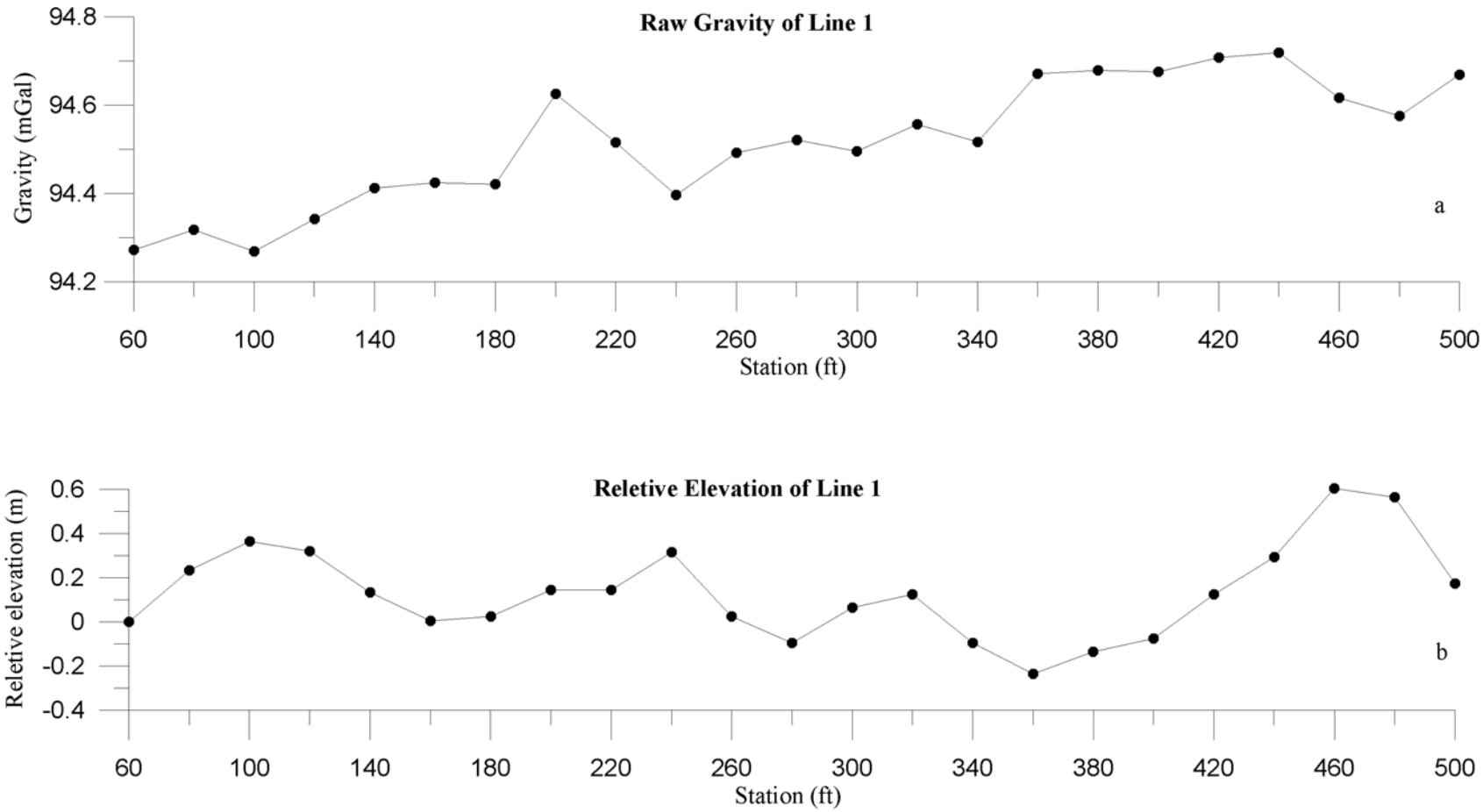

Figure 14. (a) Measured gravity data along line 1. (b) Relative elevations of line 1.

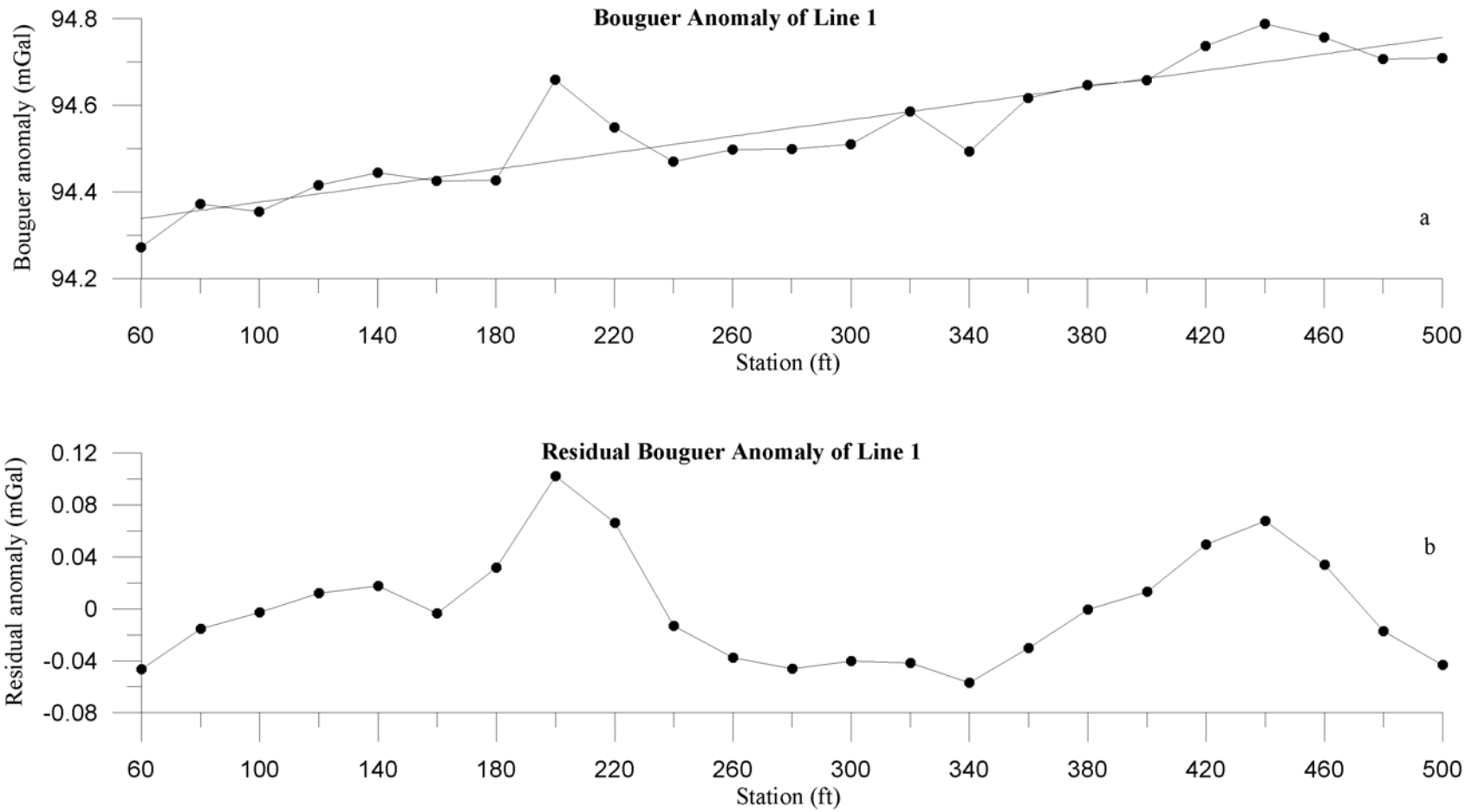

Figure 15. (a) Corrected gravity data shown by line with solid dots and the regional gravity filed shown by a straight line. (b) Residual anomalies that were calculated by removing the regional anomaly from the corrected data.

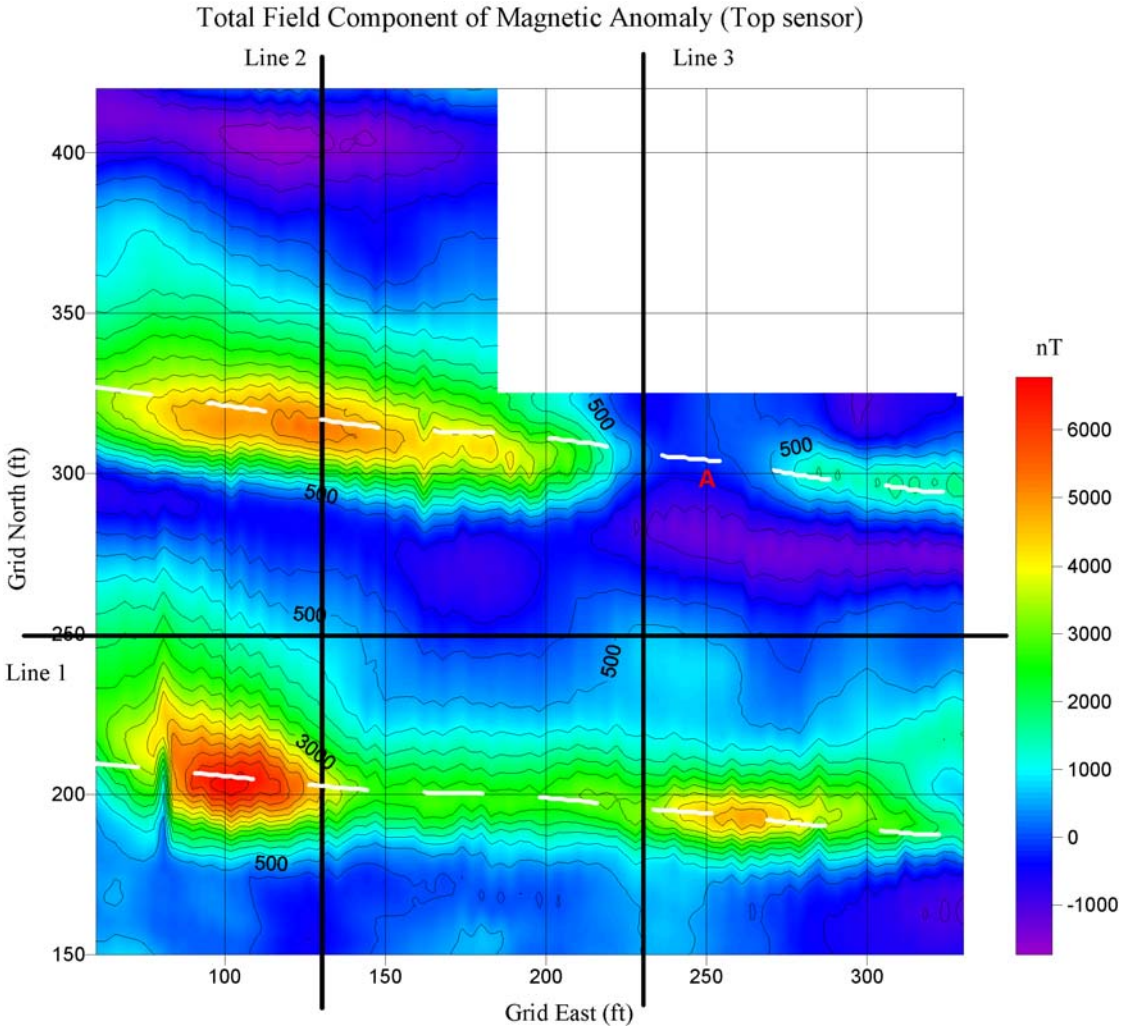

Figure 16a. The total field component of magnetic anomaly from the top sensor with interpretation.

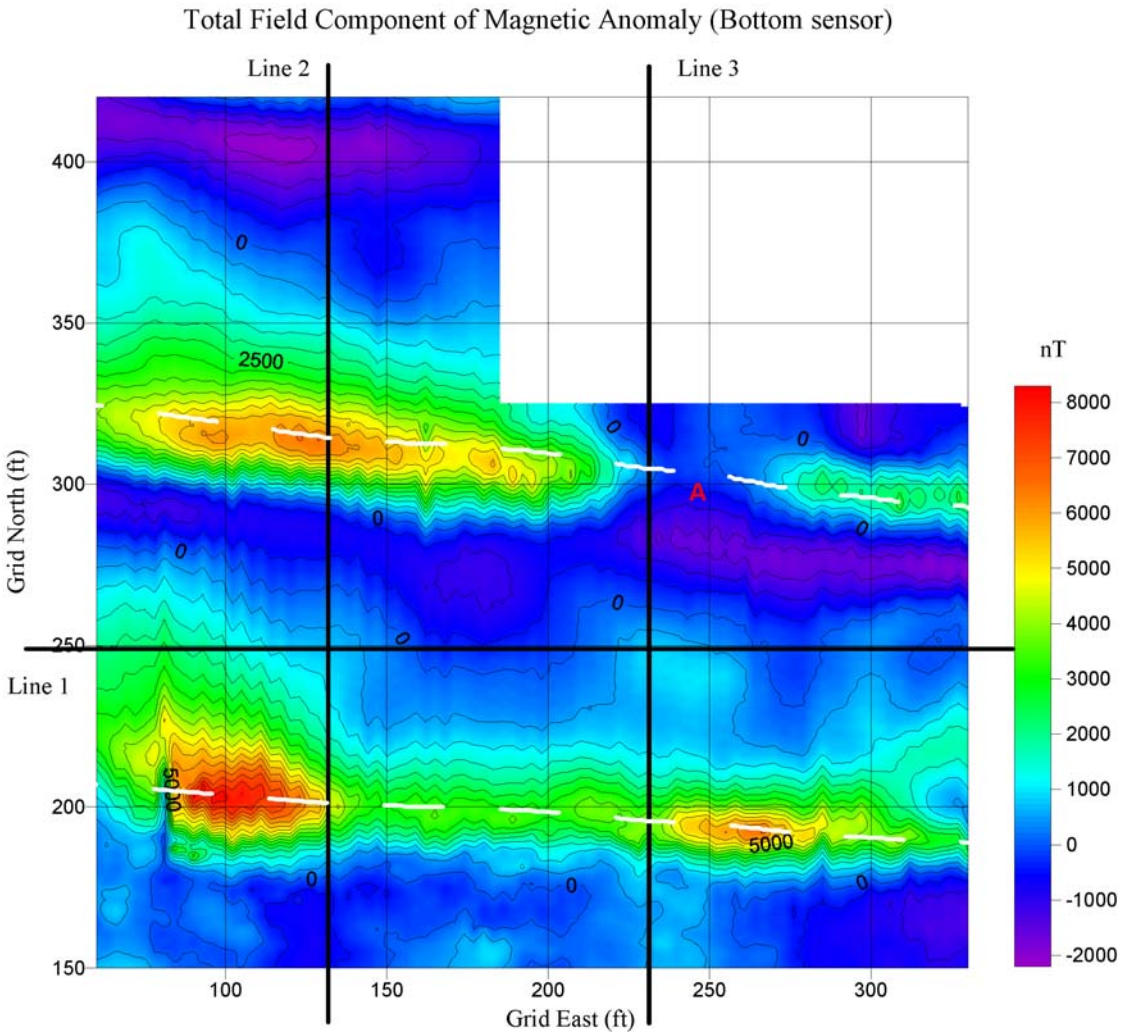

Figure 16b. The total field component of magnetic anomaly from the bottom sensor with interpretation.

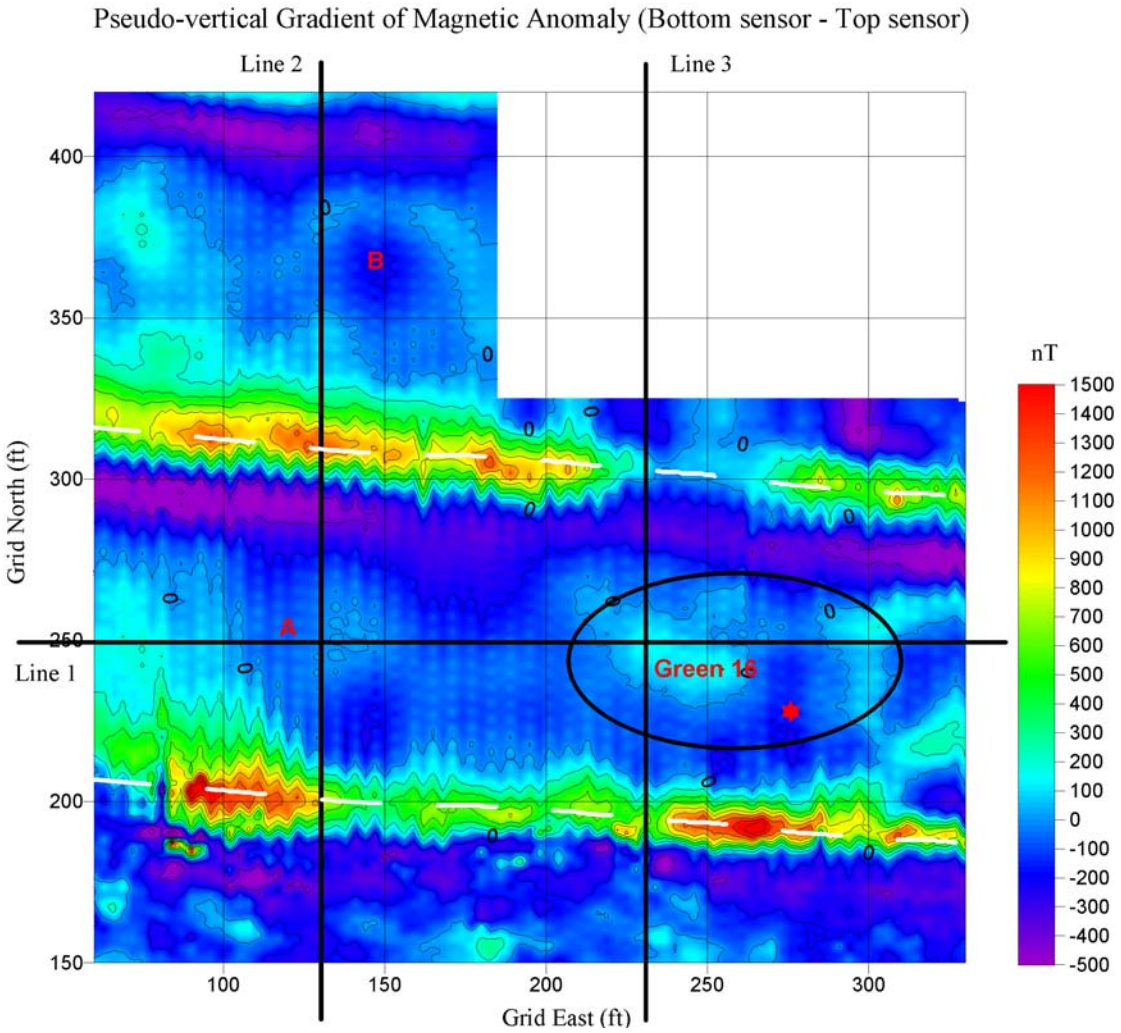

Figure 16c. The pseudo-vertical gradient of magnetic anomaly with interpretation.

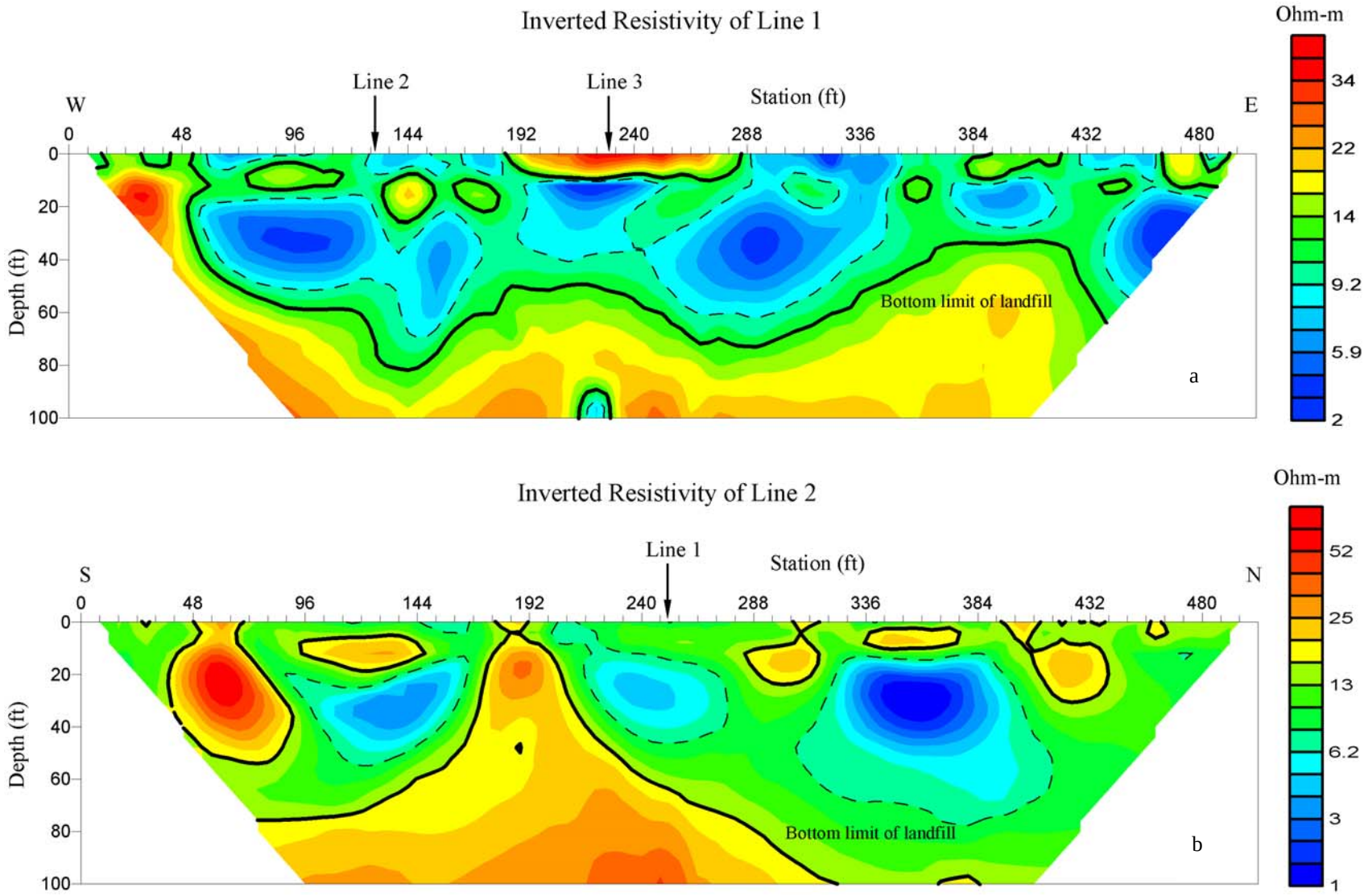
Inverted Resistivity of Line 1
Ohm-m
Line 2
Line 3
Station (ft)
W
E
0
48
96
144
192
240
288
336
384
432
480
Depth (ft)
0
20
40
60
80
100
Bottom limit of landfill
a
34
22
14
9.2
5.9
2
Inverted Resistivity of Line 2
Ohm-m
Line 1
Station (ft)
S
N
0
48
96
144
192
240
288
336
384
432
480
Depth (ft)
0
20
40
60
80
100
Bottom limit of landfill
b
52
25
13
6.2
3
1

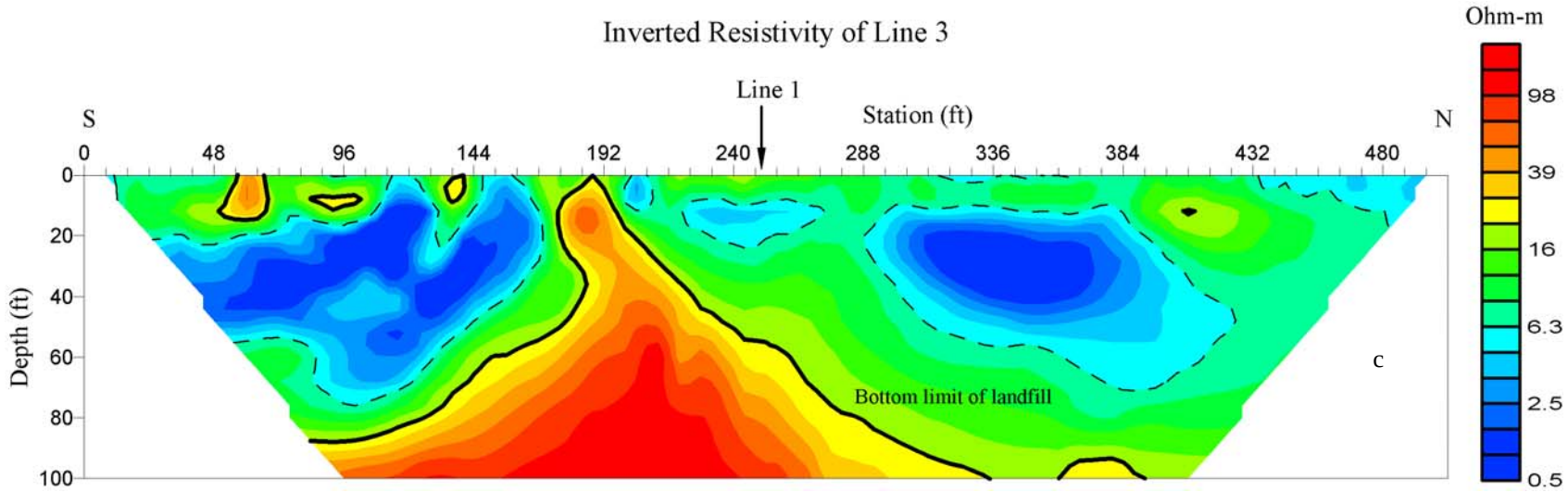

Figure 17. Inverted resistivity models with interpretation. (a) Results of line 1. Dashed lines outline bodies of landfill materials and a solid line delineates the bottom limit of the landfill. (b) Results of line 2. (c) Results of line 3.

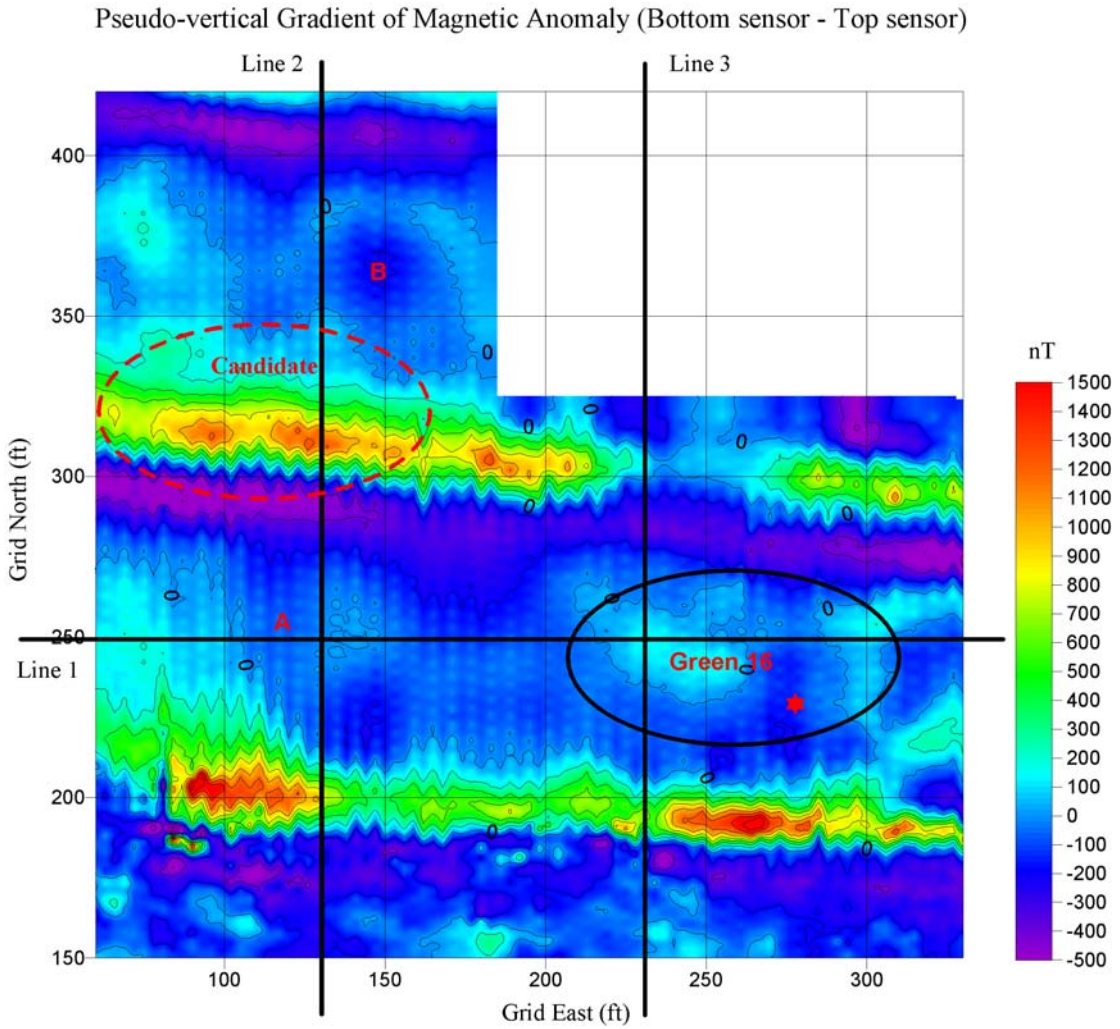

Figure 18. Recommended location for replacement of Green 16 is outlined by a dashed ellipse in red.